Global J. Environ. Sci. Manage. 13(2): xxx-xxx, Spring 2027, Serial #50

Global Journal of Environmental Science and Management
(GJESM)

Homepage: https://www.gjesm.net/

Podcasts

ORIGINAL RESEARCH ARTICLE

Flood susceptibility modeling of river overflow using an ensemble voting model

S. Sitthikankun[1], N. Suriyanon[1], C. Aryupong[2], D. Rinchumphu[1,*]

[1]Department of Civil Engineering, Faculty of Engineering, Chiang Mai University, Thailand

[2]Office of Research Administration, Chiang Mai University, Thailand

ARTICLE INFO

Article History:
Received 12 August 2026
Revised 16 October 2026
Accepted 18 November 2026

Keywords:
Ensemble learning
Flood susceptibility
Geographical information system
Machine learning
Spatial analysis

DOI:
https://doi.org/10.22034.gjesm.2027.02.03

ABSTRACT

BACKGROUND AND OBJECTIVES: Urban expansion often leads to flooding, and accurately identifying flood-susceptible areas is essential. Although machine learning algorithms are widely adopted for spatial prediction tasks, individual models frequently yield biased estimations when trained on imbalanced datasets. The study objectives were to develop a flood susceptibility prediction model for the Chiang Mai Comprehensive Plan area, Thailand, comparing four algorithms, artificial neural network, support vector machine, decision tree, and random forest, and integrating them through an ensemble voting technique.

METHODS: Field-surveyed flood marks from the October 2024 inundation event were utilized to delineate the flood boundary, which was subsequently overlaid onto 383,208 land parcel points to classify parcels as either flooded or non-flooded. Land use, land cover, elevation, slope, and distance to river were served as conditioning factors. The four models were optimized via grid search combined with five-fold cross-validation and subsequently evaluated using both an independent random test set and spatially blocked five-fold cross-validation.

FINDINGS: All models achieved comparable discrimination, with area under the receiver operating characteristic curve values ranging from 0.898 to 0.919. Under spatially blocked cross-validation, which accounts for spatial autocorrelation, the area under the curve decreased to 0.842-0.870. Each model contributes differently to the overall assessment: artificial neural network, decision tree, and random forest achieved higher sensitivity in detecting flood-susceptible areas, while support vector machine instead favored specificity over sensitivity. Integrating the predictions of all four models, the ensemble voting configuration (accuracy 0.843, recall 0.658) achieved a favorable balance between precision and specificity. Although spatial validation revealed no significant difference in discrimination between the ensemble and the leading single models, the ensemble secured second rank in four out of five folds and yielded the best-calibrated probabilities. Feature importance analysis found that elevation, land use, and distance to river are the main conditioning factors, with elevation alone accounting for approximately half of the split criteria in the tree-based models.

CONCLUSION: The developed flood susceptibility map, based on the 2024 flood event, indicates higher susceptibility concentrated along the Ping River corridor and adjacent low-lying areas. These outcomes furnish preliminary screening insights for urban planners and policymakers by isolating parcels that may necessitate site-specific flood evaluations prior to development decisions.

This is an open access article under the CC BY license (http://creativecommons.org/licenses/by/4.0/)

NUMBER OF REFERENCES	NUMBER OF FIGURES	NUMBER OF TABLES
63	6	5

*Corresponding Author:
Email: damrongsak.r@cmu.ac.th
Phone: +66 95 995 9519
ORCID: 0000-0002-6037-4974

Note: Discussion period for this manuscript open until June 01, 2027 on GJESM website at the "Show Article".

INTRODUCTION

Climate change directly affects the hydrological cycle, leading to more intense and frequent rainfall events than historical patterns. These extreme weather events are a primary cause of urban flooding and cause severe damage to human life, property, and urban economies (Dharmarathne *et al.*, 2024). Thailand is among the nations persistently affected by recurrent flooding, and in the northern region, the area defined by the Chiang Mai Comprehensive Plan exhibits significant physical susceptibility to flooding despite its predominantly mountainous surroundings. Occupying the upper floodplain of the Ping River, the site features a basin-like topography enclosed by high mountains, which is characteristic of intermontane basin settings in this region (Intarat *et al.*, 2024). These topographical features naturally turn the urban area into a catchment basin that receives runoff from the surrounding mountainous terrain. The region has experienced repeated catastrophic floods, including major inundations in 2011 (Gu *et al.*, 2025) and, more recently, in early October 2024, when the Ping River overflowed its banks after heavy seasonal rainfall, prompting evacuations and widespread inundation across the city. Although the severity of the 2024 event was driven primarily by this overflow, inundation was not confined to riparian zones, as several municipal areas also experienced sudden flooding (Leelawat *et al.*, 2025). Riverine flooding transpires when excessive catchment precipitation surpasses the discharge capacity of the principal channel, whereas urban waterlogging typically manifests in municipalities characterized by extensive flood-susceptible zones (Damayanti *et al.*, 2024). In Chiang Mai, urban expansion (Prasertsoong and Puttanapong, 2025) has replaced high-water-retention land uses, such as paddy fields and green spaces, with impervious surfaces, a process shown to significantly reduce regional water retention capacity and elevate flood risk (Gu *et al.*, 2025). When riverine flooding and urban waterlogging occur simultaneously, the severity of the inundation is further amplified. Proactively identifying flood-susceptible areas prior to urban expansion enables planners to delineate restricted-development zones and target protective interventions for existing infrastructure; consequently, integrating flood exposure data into comprehensive land-use plans is widely recommended (Puno *et al.*, 2021). A reliable flood susceptibility model requires an accurate flood inventory to serve as the dependent variable. Hydrodynamic models can generate simulated flood maps for training machine learning models (Bentivoglio *et al.*, 2022), but they require high-resolution input data and extensive computation (Panyadee and Champrasert, 2024), their accuracy depends heavily on topographic data quality (Alexopoulos *et al.*, 2025), and models calibrated for one city often fail to generalize to others (Krishnachaithanya *et al.*, 2025). Remote sensing offers an alternative for large areas; for example, Wu *et al.* (2023) combined Sentinel-1 Synthetic Aperture Radar (SAR) data with deep learning for near-real-time flood delineation, overcoming cloud cover. However, satellites possess fixed revisit intervals and fail to capture continuous imagery of identical location (Wu *et al.*, 2023), furthermore, in densely built urban areas, SAR signals are distorted by double-bounce scattering from tall structures and reflective roofs (Krishnachaithanya *et al.*, 2025). Unmanned Aerial Vehicles (UAV) provide higher resolution but are limited by heavy rain, strong winds, short battery life, and restricted flight zones during floods (Wienhold *et al.*, 2023). In contrast, field surveys integrating flood marks combined with Global Positioning System (GPS) coordinates directly capture on-the-ground conditions furnish reliable ground truth for model training (Khosravi *et al.*, 2019; Wüthrich *et al.*, 2025), although such methods are labor-intensive and must be conducted promptly following a flood event

before the high-water marks fade (Notti *et al.*, 2018). Traditional methods based on expert opinion are prone to subjective bias in assigning factor weights (Usman Kaoje *et al.*, 2021). In contrast, machine learning (ML) is widely recognized for its ability to analyze complex, non-linear relationships among physical factors (Panyadee and Champrasert, 2024; Tochaiwat and Pultawee, 2024). Seydi *et al.* (2023) showed that support vector machine (SVM), decision tree (DT), random forest (RF), and ensemble models can classify flood-prone areas with high accuracy. Similarly, Duwal *et al.* (2023) found artificial neural network (ANN), SVM, and RF effective in a river basin with complex topography, and Bhattarai *et al.* (2024) demonstrated the reliability of ANN and SVM in predicting flood-prone areas. In a Thai urban context, Srivanit *et al.* (2024) applied multiple ML classifiers to urban form indicators, revealing that a bagging decision tree model most accurately replicated flood-susceptible zones derived from a governmental flood simulation model. Nevertheless, relying exclusively on a single methodological approach can compromise predictive accuracy (Rachmawardani *et al.*, 2025). Standalone algorithms such as DT or neural networks often exhibit an imbalanced bias-variance trade-off (Saleh *et al.*, 2024) and are prone to local optima, resulting in lower predictive performance than multi-model approaches (Abu-Salih *et al.*, 2023). Ensemble learning addresses these limitations by integrating the predictions of multiple models. Saleh *et al.* (2024) reported that a boosting ensemble combining SVM, k-nearest neighbors, and DT achieved 98.75 percent (%) accuracy, outperforming individual approaches, and Abu-Salih *et al.* (2023) applied optimized ensemble learning to flood risk in road networks, achieving an area under the receiver operating characteristic curve (AUC) of 0.90. Furthermore, integrating multiple models has been demonstrated to enhance flood prediction accuracy compared to single algorithms (Choubin *et al.*, 2019) while mitigating individual model biases in urban flood hazard prediction (Taromideh *et al.*, 2024). Within the Chiang Mai Comprehensive Plan Area, flood susceptibility information at the scale of individual land parcels, derived from field-verified flood evidence, remains limited. In addition, ML susceptibility models are often evaluated with random train–test splits, which can overestimate predictive performance when neighboring samples are spatially autocorrelated (Roberts *et al.*, 2017). Accordingly, this study addresses three primary research questions: 1) To what extent can ML models, driven by five physical conditioning factors, accurately predict flood-susceptible land parcels? 2) How does an ensemble soft voting model compare to individual base models in identifying these parcels under both random and spatially blocked validation frameworks? 3) Which conditioning factors exert the greatest influence on flood susceptibility, and how are susceptibility levels distributed across the statutory land-use zones defined in the comprehensive plan? The aim of the current study is to develop a flood susceptibility prediction model by comparing ANN, SVM, DT, and RF and integrating them through ensemble soft voting, using field-surveyed flood evidence from the 2024 event, to evaluate the models with spatially blocked cross-validation, and to provide a parcel-level flood susceptibility map as one of several references for urban planning and land-use management. This study has been carried out in the Chiang Mai Comprehensive Plan Area, Thailand, in 2024-2026.

MATERIALS AND METHODS

Study area

The study area is the Chiang Mai comprehensive plan area, a major economic and tourism hub of northern Thailand. The old city, a historically and culturally significant area within the plan boundary, has substantial potential as a model for creative tourism and cultural heritage conservation (Hongnual *et al.*, 2021). The Chiang Mai Comprehensive Plan zones land use to

regulate development, promote conservation, and accommodate urban growth (Fig. 1). Enclosed by the Chiang Mai moat, the urban core serves as a designated conservation zone intended to foster cultural and artistic identity (light brown zone). This square-shaped precinct encompasses a diverse mix of educational institutions, temples, commercial complexes, and residential developments. Adjacent to this core is the commercial and high-density residential zone (red zone), characterized by a substantially high proportion of impervious surfaces. Further outward, urban expansion areas along the second and third ring roads are designated as medium-density (orange zone) and low-density (yellow zone) residential zones. The peripheral zones consist predominantly of agricultural and rural terrain (green zone), safeguarding open space at the urban boundary, whereas zones dedicated to governmental facilities (blue zone) and educational institutions (olive- green zone) are interspersed throughout the study area (Ministry of Interior, 2012).

Methods

The methodology was structured into three distinct phases: 1) data collection and geographic information system (GIS) processing, 2) ML model development and overfitting checks, and 3) ensemble modeling and spatial integration. All spatial data were processed in quantum geographic information system (QGIS), an open-source GIS software, and flood boundaries and land parcels were stored in polygon vector format to allow overlay analysis with other vector layers (Verma *et al.*, 2024).

Data collection and spatial database

The data collection and spatial database preparation comprised three primary components: 1) field surveys to determine the actual flooded area boundaries, 2) flood susceptibility factors functioning as independent variables, and 3) land plot maps serving as the foundational database for identifying parcel-level susceptibility. All collected data were analyzed through GIS processing and overlay analysis to generate datasets for model development, as illustrated in Fig. 2.

Field survey

This study used field survey data on flood marks to collect flood boundary data for 2024, as part of the Urban Flood Warning Information System Project in Chiang Mai Province (Center of Excellence in Natural Disaster Management, 2024). The procedure commenced through coordination with local municipal disaster prevention and mitigation agencies, enabling local officials to assist in identifying and mapping actual inundation zones within the respective sub-districts to secure comprehensive data on the affected areas. The recording process proceeded as follows: 1) location recording, which involved assigning measurement point codes, documenting administrative details (village, village number, sub-district, district, province), and acquiring latitude and longitude coordinates via GPS devices for precise spatial identification; 2) measuring depth levels based on flood marks appearing on electricity poles using an optical level, establishing the road surface level at the base of the pole as the reference criterion at +0.000 meters; 3) clearly marking the maximum flood level (flood mark) on the electricity poles to serve as reference points; 4) recording all survey data, encompassing measurement point codes, coordinates, and depth level values, to be entered and compiled into a database system for subsequent analysis; and 5) utilizing field-recorded location coordinates and water depths to delineate actual flood boundaries on Google Maps to visualize the overall inundation extent, subsequently exporting digitized boundaries to GIS to generate a spatial data layer for overlay analysis alongside susceptibility factors. The resulting 2024 flood inventory map, which served as the basis for labeling the dependent variable, is shown in Fig. 3.

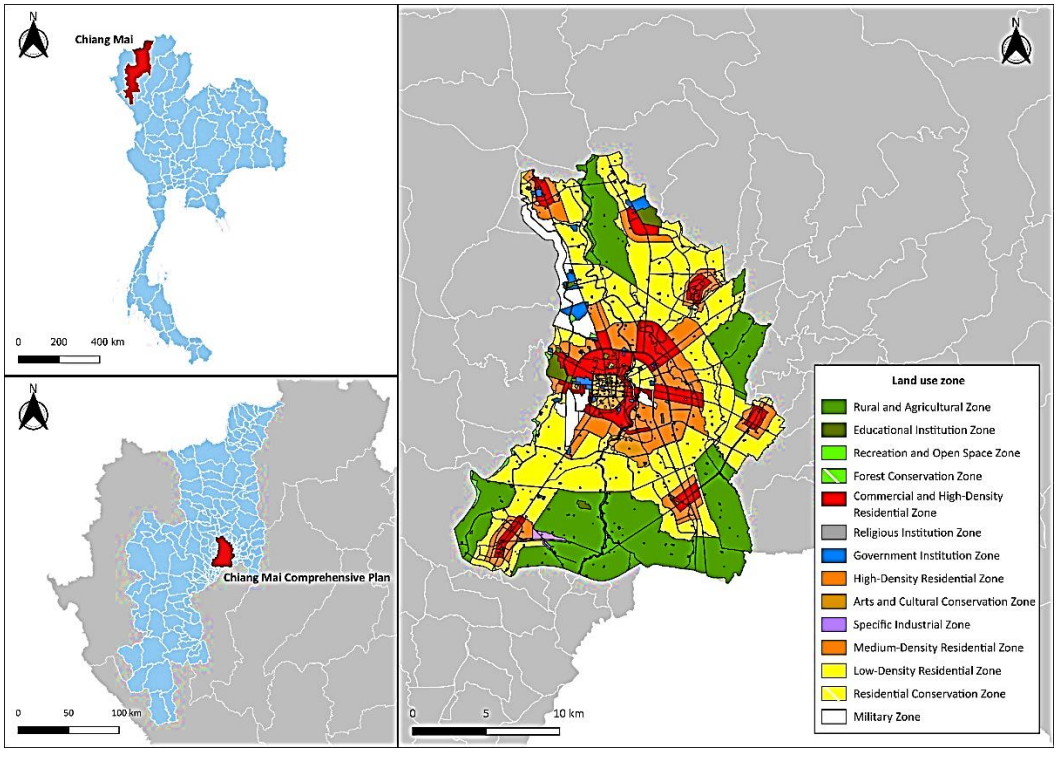

Fig. 1: Geographical location of the study area and land use of the Chiang Mai comprehensive plan area in Thailand (Ministry of Interior, 2012)

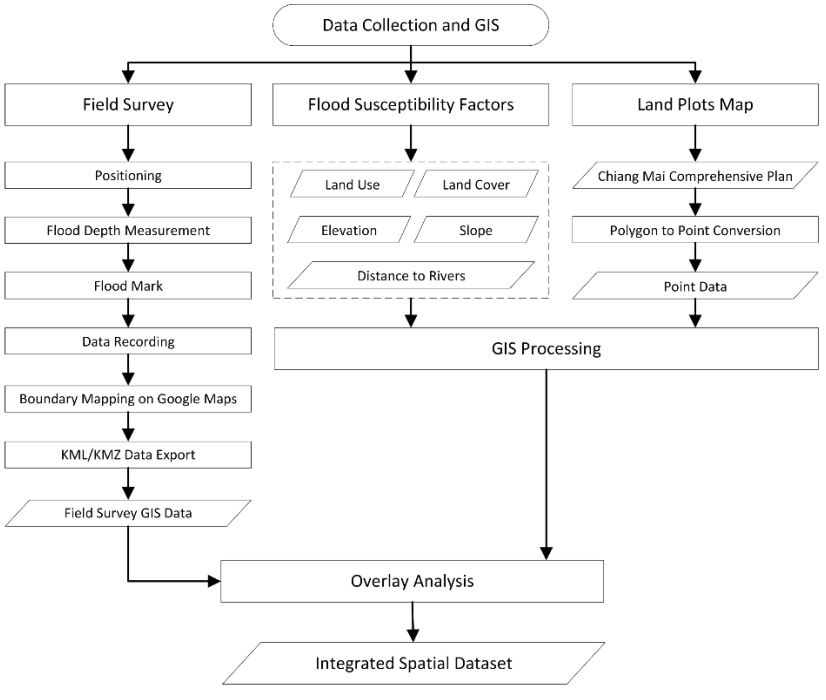

Fig. 2: Data collection and GIS framework

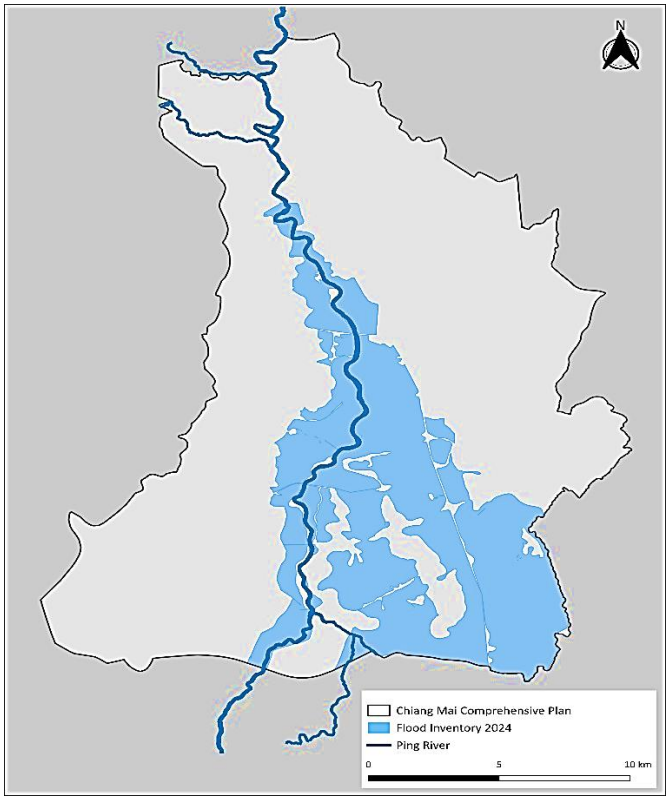

Fig. 3: Flood inventory map of the Chiang Mai Comprehensive Plan area in 2024

In total, 4,711 flood-mark points were recorded between October 2024 and May 2025. Because the flood boundary was delineated from discrete flood-mark locations, parcels near the boundary are subject to positional uncertainty, which was not quantified in this study and is acknowledged as a limitation.

Flood susceptibility factors

To establish the spatial conditioning variables influencing flood susceptibility, data layers representing five primary factors were acquired and processed from multiple authoritative sources: 1) Land Use involves extracting and reclassifying statutory land-use boundary data based on the color-coded zoning regulations of the Chiang Mai Comprehensive Town Planning Law (Ministry of Interior, 2012); 2) Land Cover data for 2024 were obtained from the Google Dynamic World (V1) dataset via Google Earth Engine (GEE). Derived from Sentinel-2 imagery at a 10-meter spatial resolution using a deep learning fully convolutional neural network (FCNN) with a reported overall agreement of 73.8% (Brown *et al.*, 2022), the dataset was reclassified into three hydrologically relevant classes: impervious surface, pervious surface, and water surface; 3) To align spatial grids across model inputs, topographic records were queried from the National Aeronautics and Space Administration digital elevation model (NASADEM) product (Crippen *et al.*, 2016) accessed via GEE, resampling the native 30-meter cells to 10 meters upon export. Prior research shows that digital elevation model (DEM) choice and grid spacing shape flood hazard mapping outcomes (Puno *et al.*, 2022); yet resampling cannot recover sub-grid relief—meaning effective terrain detail stays anchored to the 30 meters base layer and fine micro-topographic features in small parcels remain

coarsely represented; 4) Slope was determined by analyzing the 10-meter resampled DEM data using spatial analysis tools in QGIS to calculate the area's slope percentage; and 5) Distance to River was generated by delineating the primary Ping River network and creating multi-ring buffers at 1-kilometer (km) intervals in GIS, assigning each location to a distance class from 1 (within 1 km) to 8. In the concluding preprocessing step, co-registration and spatial overlay were executed across all five raster layers within a GIS platform to sample uniform biophysical metrics across the study domain, generating the explanatory inputs (X1–X5) passed into the ML training stage. These factors were selected based on a study by Sitthikankun *et al.* (2024), which used a systematic literature review guided by the Preferred Reporting Items for Systematic Reviews and Meta-Analyses (PRISMA) framework to identify the variables commonly used to predict urban flooding. Among these variables, factors that could be obtained readily from open or publicly available sources were selected, so that the approach can be reapplied using readily available data, and a small set of variables was preferred to keep the model simple. Several relevant catchment and hydrometric factors, namely rainfall intensity, river discharge, drainage capacity, drainage density, soil properties, flow accumulation, and topographic wetness, fell outside the scope of this analysis, leaving their non-inclusion to be evaluated among the study limitations. Land use reflects urban transformation, as highly urbanized areas dominated by impervious surfaces reduce permeability and increase surface runoff (Faksomboon *et al.*, 2025), and inappropriate development in flood-prone areas increases the concentration of susceptible locations (Rentschler *et al.*, 2023). Land cover influences infiltration capacity, as the replacement of vegetated zones by built environments degrades soil infiltration (Tang *et al.*, 2024). Terrain height highlights valley floors and depressed basins exposed to frequent flood events (Gohil *et al.*, 2024), landscapes increasingly encroached upon by present-day city growth (Rentschler *et al.*, 2023). Slope controls water velocity and the time of concentration, with flat terrain restricting drainage and prolonging inundation, and must be analyzed alongside elevation (Gohil *et al.*, 2024). Distance to river reflects the likelihood of overbank flow, as riparian zones are the first affected during peak discharge (Saleh *et al.*, 2024) and often serve as natural drainage pathways where surrounding runoff converges (Yaseen, 2024). Screening for predictor collinearity, a condition capable of inflating feature redundancy and skewing variable importance rankings, was conducted by computing variance inflation factors (VIF) across all five inputs using the conventional threshold of 5 (Abdo *et al.*, 2025). Because land use and land cover are categorical variables entered into the models as integer codes, the generalized VIF (GVIF) was also calculated with both variables represented as dummy variables $GVIF^{\frac{1}{2df}}$, where; df is the number of dummy variables of a factor, is comparable to the square root of the VIF and was therefore compared with $\sqrt{5} \approx 2.24$ (Fox and Monette, 1992; Tuganishuri *et al.*, 2025).

Land parcel processing and target variable labeling

The spatial baseline dataset used in this research was derived from the official cadastral land plots map covering the entire Chiang Mai Comprehensive Plan boundary, provided in polygon vector format. To enable ML modeling at the parcel level, a polygon-to-point conversion technique was applied in QGIS to extract the geometric centroid of each land parcel, creating discrete representative parcel points across the study area. Following that step, point-in-polygon matching was carried out to pair the sample parcel coordinates with the observed 2024 flood footprint compiled from ground surveys. The spatial intersection was transformed into a binary dependent target variable (Y), where parcel points falling within the recorded flood boundary

were designated as flooded (Y = 1). Conversely, locations lying beyond the mapped flood extent received a Non-flooded label (Y = 0). Parcels labeled Y = 0 were not inundated during the 2024 event but are not necessarily free from flooding under other hydrological conditions. Representing entire land units by a single center point meant that flood status for partially submerged properties depended purely on whether that point fell inside the water boundary, introducing potential labeling errors for expansive or complex-shaped lots. In this study, flood susceptibility refers to the relative likelihood of parcel inundation given its physical and land-use conditions; it does not incorporate flood intensity (hazard) or exposure and vulnerability (risk). This binary assignment strategy aligns with established flood hazard modeling methodologies (Choubin *et al.*, 2019; Taromideh *et al.*, 2024) and establishes the labeled spatial inventory dataset for subsequent conditioning factor extraction and model training. Binary labeling of flooded (1) and non-flooded (0) locations is widely used to prepare datasets for ML models (Hong *et al.*, 2018; Yu *et al.*, 2023). Class imbalance, where inundated parcels occur far less frequently than non-inundated ones, undermines overall accuracy as a standalone metric, since classifiers can achieve high scores simply by defaulting to the dominant category (Khalid and Khan, 2024; Wang *et al.*, 2024). Model performance was therefore evaluated with metrics suitable for imbalanced data, specifically precision, recall, F1-score, and AUC, with emphasis on the flood-susceptible class (Ekmekcioğlu *et al.*, 2022; Rahmati *et al.*, 2019). With a class proportion near 1:2.78 indicating only moderate skew, oversampling, under sampling, and sample weighting were left out; stratified fold generation and distribution-aware performance measures served in their place to preserve the original class distribution and ensure reliable model evaluation across minority and majority classes while minimizing potential evaluation bias under the observed class distribution.

Machine learning model development

All data preprocessing, ML model development, hyperparameter optimization, and ensemble soft voting frameworks were implemented in Python (version 3.11). Model training and evaluation routines used Scikit-learn (v1.7) for the SVM, DT, and RF algorithms, alongside TensorFlow/Keras (v2.21) for the ANN architecture. The geospatial data abstraction library/ OGR simple features library (GDAL/OGR), integrated with QGIS, performed spatial vector-to-point transformations and sampled raster features. Consistent replication across dataset division and model fitting was a core design priority throughout the experimental procedure. Hierarchical partitioning across two levels structured the dataset division to curb overfitting and promote strong performance on held-out observations, depicted in Fig. 4. Four diverse base estimators, each relying on a different algorithmic foundation, were combined within the ensemble. ANN mimics the structure of biological neural networks, passing input features through one or more hidden layers of weighted neurons and adjusting the weights through backpropagation to capture non-linear relationships (Khudhair *et al.*, 2024). SVM constructs an optimal hyperplane that maximizes the margin between classes, using kernel functions such as the radial basis function (RBF) to separate non-linear data (Tehrany *et al.*, 2014). DT partitions data through sequential decision rules based on criteria such as the Gini index, providing interpretable results but tending to overfit when trees grow excessively deep (Usman-Hamza *et al.*, 2025). Expanding on single-tree DT models, RF applies bootstrap resampling paired with randomized predictor selection across many constituent trees, pooling their predictions to temper variance and restrain overfitting while improving predictive stability across datasets and enhancing generalization to unseen observations under diverse data conditions and varying predictor interactions and relationships (Usman-Hamza *et al.*, 2025).

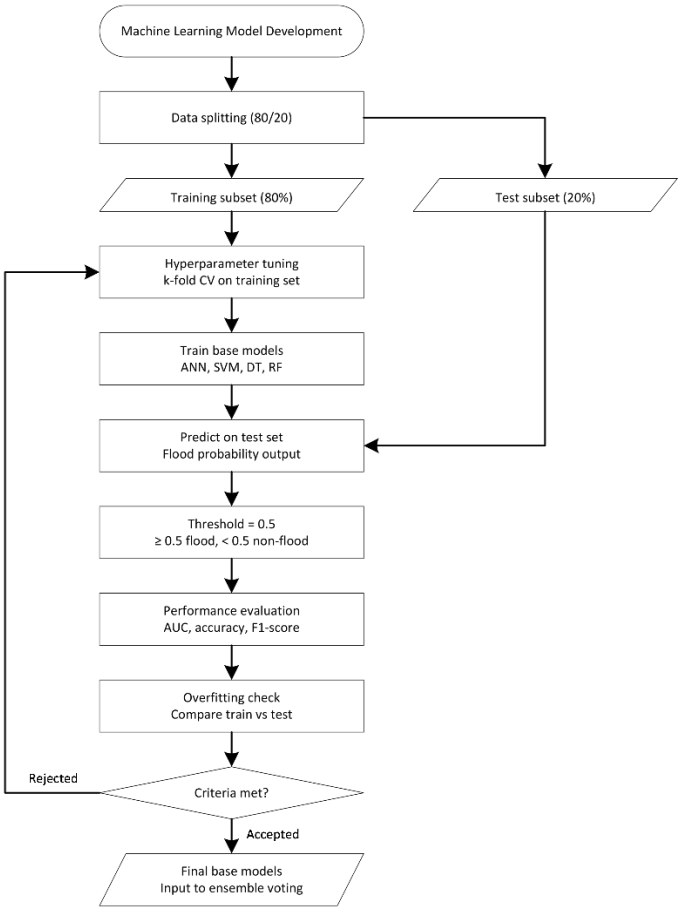

Fig. 4: Machine learning and overfitting check framework

Data splitting and validation

Ahead of training the algorithms, gaps in feature attributes across the sampled parcel locations were completed with per-variable mean values so the analytical table remained uniform. Assigning integer labels to land use and land cover categories applied uniformly across every model, and scaling all inputs via z-score transformation relied solely on training-partition moments to prevent information leakage. A common data-partitioning protocol then divided the complete dataset (n = 383,208) into an 80% training set (306,566 samples) and an independent 20% testing set (76,642 samples). Stratified random sampling was applied to maintain the empirical class distribution between flood-susceptible parcels (26.47%, Class 1) and non-flooded parcels (73.53%, Class 0) across both partitions. To ensure computational stability and complete reproducibility, all randomized procedures, including sample splitting, cross-validation folds, and tree bootstrapping, were anchored to a fixed random seed (random state = 42). Retaining a fixed three-way division was bypassed so model fitting could draw from as much training data as possible while guarding against overfitting on skewed classes; evaluation on the 80% training share relied instead on 5-fold stratified cross-validation. The training pool was iteratively partitioned into five stratified subsets, using four folds for model fitting and hyperparameter optimization, while the remaining fold served for

internal validation. This method avoided the sample loss of an explicit validation split and minimized the evaluation variance of a single arbitrary partition, providing stable performance baselines before final testing. Testing model transfer across geographic zones, and curbing inflated accuracy estimates triggered when neighboring parcels share spatial dependence under random division (Roberts *et al.*, 2017), motivated a supplementary spatially blocked five-fold cross-validation. The study area was divided into 2 km × 2 km blocks (128 blocks containing parcels), and whole blocks were assigned to folds by stratified group k-fold partitioning, so that parcels in the same block never appeared in both the training and validation sets. In each fold, every model was retrained with the optimal hyperparameters from the grid search, with imputation and scaling fitted on the training folds only and with SVM trained on a 30% stratified subsample of the training folds, as in the main analysis; the soft voting ensemble was then recomputed from the out-of-fold probabilities. Statistical comparisons of AUC gaps between the combined model and every standalone learner relied on 1,000 block-bootstrap iterations over 2 km spatial tiles, capturing local spatial correlation across neighboring parcels. Probability calibration was assessed with the Brier score, the expected calibration error (ECE, 10 equal-width bins), and a comparison of the mean predicted probability with the observed flood rate in each susceptibility level. Performance-weighted (AUC − 0.5) and reduced-model ensemble alternatives were compared with equal-weight soft voting using the same out-of-fold probabilities.

Model training and performance evaluation

Four supervised ML algorithms were trained to predict flood susceptibility: ANN, SVM, DT, and RF. Hyperparameters were systematically tuned using grid search combined with 5-fold stratified cross-validation on the training set, evaluated by mean AUC and its standard deviation across folds. Candidate hyperparameter grids were defined across all four classifiers: for the ANN, hidden-layer widths of (16, 8), (32, 16), and (64, 32), step sizes (learning rates) of 0.01 and 0.001, and batch sizes of 32 and 64; for the DT, depth ceilings of 5, 10, 15, or none, leaf sample floors of 1, 5, or 10, split sample floors of 2 or 10, and Gini or entropy split rules; for the RF, tree counts of 100 or 300, depth ceilings of 10, 20, or none, leaf sample floors of 1 or 5, and square-root or log2 feature counts; and for the SVM with a radial basis function kernel, C values of 0.1, 1, and 10 with gamma values of scale, 0.01, and 0.1. The selected settings were 64 and 32 hidden units, a learning rate of 0.001, and a batch size of 32 for ANN; unlimited depth, 5 samples per leaf, 10 samples per split, and the Gini criterion for DT; 300 trees, a maximum depth of 20, 5 samples per leaf, and log2 feature sampling for RF; and C = 10 and gamma = scale for SVM. The ANN comprised two fully connected hidden layers with rectified linear unit activation and a two-unit SoftMax output layer, and it was trained with the Adam optimizer and categorical cross-entropy loss for up to 100 epochs, with early stopping on validation loss (patience of 8 epochs on the validation fold during tuning and 10 epochs on a stratified 10% subset of the training set for the final model). The SVM model used an RBF kernel to classify non-linear flood boundaries. High runtime and memory costs prohibited running SVM training across all available records, so parameter estimation and tuning relied instead on a class-stratified draw of 91,969 observations (~30% of the training pool). This subsample size was determined through a two-stage learning curve analysis to reach AUC and F1-score stabilization. The remaining three models (ANN, DT, and RF) were trained on the complete 80% training set (306,566 samples). All models were evaluated on the 20% test set (76,642 samples) using a 0.5 decision threshold. Model performance was measured using accuracy, precision, recall, specificity, F1-score, AUC, Cohen's Kappa, and Matthews Correlation Coefficient (MCC). Permutation feature importance (mean AUC decrease across 10

repetitions) was calculated on the test set for all models, alongside Mean Decrease in Impurity (MDI; Gini importance) for DT and RF. Close agreement between cross-validation and test AUC results, separated by less than 0.01 across all four learners, indicated minimal overfitting risk, supporting the inclusion of every model in soft-voting ensemble aggregation.

Ensemble soft voting

Ensemble learning combines multiple predictive models rather than relying on a single estimator to reduce variance, mitigate overfitting, and improve predictive stability. Bagging averages estimators trained on bootstrap samples to reduce variance, boosting sequentially corrects the errors of preceding learners to reduce bias (Zhao *et al.*, 2025), and stacking uses a meta-learner to weight heterogeneous base models (Nguyen Van and Lee, 2025). Combining predicted class likelihoods from individual estimators via soft voting delivers an interpretable, straightforward strategy tailored to mapping spatial susceptibility. In soft voting, the probability levels generated by each model are averaged rather than counting only discrete class votes (Wara *et al.*, 2025; Yang *et al.*, 2024), and combining model predictions in this way has been shown to reduce prediction variance and individual algorithmic bias in flood susceptibility mapping (Choubin *et al.*, 2019; Taromideh *et al.*, 2024). Once parameter tuning concluded, class-probability estimates from all four constituent classifiers were pooled by soft voting, taking the arithmetic mean across learners to produce a continuous flood susceptibility assessment, using Eq. 1 (Talha *et al.*, 2025):

$$P_{soft}(x) = \frac{1}{N}\sum_{i=1}^{N} P_i(x) \quad (1)$$

Where: $P_i(x)$ is the predicted probability of the flood-susceptible class (Class 1) generated by the i-th base model for feature vector x, and N = 4. Equal weights were assigned because the base models had similar cross-validation AUC values (0.893-0.917); performance-weighted and reduced-model alternatives were compared under spatial cross-validation. Class labels were assigned at a threshold of 0.5. The averaged probability was classified into five susceptibility levels using the equal interval method: Very Low (0.000-0.200), Low (0.200-0.400), Moderate (0.400-0.600), High (0.600-0.800), and Very High (0.800-1.000). Five-level classification is widely adopted in flood susceptibility studies because it supports spatial prioritization (Abraham *et al.*, 2021; Narendra *et al.*, 2024; Pradhan *et al.*, 2023), although three- and four-level schemes are also used (Chowdhuri *et al.*, 2020). Equal interval classification was selected over Jenks natural breaks to preserve the absolute meaning of the predicted probabilities, because with a dataset dominated by Class 0, data-dependent methods would shift class boundaries downward and classify moderate-probability areas as highly susceptible. Lacking post-hoc probability calibration, the mean ensemble outputs serve as comparative flood-susceptibility indicators instead of literal likelihoods of future flood occurrence.

Spatial integration and final mapping

Resulting soft-voting scores were mapped onto the study area during spatial post-processing to assemble the final flood-susceptibility layer. The continuous susceptibility probabilities and their corresponding five-level susceptibility categories were linked back to the cadastral parcel spatial database by joining the representative sample points to their respective land parcel polygons via unique cadastral identifiers (ID). The resulting geospatial layer was exported as a GeoPackage and subsequently imported into QGIS for cartographic symbolization. Carrying out these steps established the parcel flood-susceptibility map, capturing how susceptibility shifts across five risk gradations across the Chiang Mai Comprehensive Plan extent, thereby supporting spatial prioritization and flood-risk management.

RESULTS AND DISCUSSION

This section presents the flood inventory, multicollinearity analysis, model performance, spatial cross-validation, flood susceptibility map, and feature importance results.

Flood inventory analysis

The dataset comprised 383,208 representative land parcel points, of which 101,420 (26.47%) fell within the 2024 flood boundary (Class 1) and 281,788 (73.53%) fell outside it (Class 0), a ratio of approximately 1:2.78. Skewed category counts reveal uneven class representation, consistent with the class imbalance frequently encountered in flood and disaster records.

Multicollinearity analysis

Multicollinearity among the five conditioning factors was examined to avoid redundancy that could distort the feature importance analysis (Abdo *et al.*, 2025; Rahman *et al.*, 2025). As shown in Table 1, all VIF values ranged from 1.016 to 1.120, well below the threshold of 5, indicating that the factors were sufficiently independent for model training. Categorical treatment of land use and land cover prompted a check of the GVIF alongside standard collinearity diagnostics; $GVIF^{\frac{1}{2df}}$ ranged from 1.008 to 1.100, well below $\sqrt{5}$ (≈ 2.24), and the association between land use and land cover was weak (Cramér's V = 0.148). The multicollinearity assessment was therefore robust to the encoding of the categorical variables.

Model performance comparison

Benchmarking all five models on the held-out test split measured how reliably each separated flood-prone parcels from non-susceptible ones. The results, evaluated based on accuracy, precision, recall, specificity, F1-score, AUC, Cohen's Kappa, and MCC, are presented in Table 2. An evaluation of the individual base models reveals distinct operational characteristics across algorithms. Tree-based models achieved marginally higher discriminative capacity than the other single models; RF achieved an AUC of 0.9194, closely followed by DT (AUC = 0.9187) and ANN (AUC = 0.9170). RF, DT, and ANN exhibited balanced sensitivity, yielding Class 1 recall values of 0.7066, 0.7047, and 0.7021, respectively. Conversely, SVM yielded comparatively lower detection metrics (accuracy = 0.8321, AUC = 0.8982, and Class 1 recall = 0.6195), indicating that its decision boundaries on large-scale geospatial distributions leaned toward the non-flooded majority class. Pooling predictions through soft voting drew together the complementary forecasting patterns of all four base classifiers. While standalone RF attained a marginally higher AUC, the ensemble achieved the highest Class 1 precision (0.7223) and the highest specificity (0.9089, only marginally above SVM's 0.9087). As shown by the confusion matrix, the ensemble limited false positives to 5,132 instances, compared with 6,093 in ANN and 5,971 in RF. Fewer false-positive designations help limit unneeded secondary flood reviews on parcels unlikely to flood, though stronger precision and specificity traded off against sensitivity, leaving ensemble Class 1 recall (0.6582) behind RF, DT, and ANN because SVM's weaker flood-detection rate weighed on the unweighted mean. This precision-recall trade-off indicates that each model offers a different prediction profile: RF, DT, and ANN favor the detection of flood-susceptible parcels, whereas the ensemble favors fewer false alarms. The AUC values obtained in this study (0.898-0.919) are comparable to those reported in previous flood susceptibility studies, such as Choubin *et al.* (2019) (AUC = 0.91) and Abu-Salih *et al.* (2023) (AUC = 0.90). Unlike Saleh *et al.* (2024), who reported that an ensemble model clearly outperformed individual approaches, the ensemble in this study performed comparably to the strongest single models in overall discrimination. Strong baseline accuracy from the individual tree-based learners on this dataset likely accounts for the modest margin left for probability averaging to improve upon, particularly under classification conditions.

Table 1: Variance inflation factor and generalized variance inflation factor values of flood conditioning factors

Factors	VIF	$GVIF^{\frac{1}{2df}}$
Elevation (X3)	1.120	1.100
Distance to river (X5)	1.068	1.062
Slope (X4)	1.040	1.021
Land use (X1)	1.025	1.008 (df = 12)
Land cover (X2)	1.016	1.012 (df = 2)

Table 2: Performance of individual base models and the ensemble soft voting model on the independent test set

Model	Accuracy	Precision (Class 0)	Precision (Class 1)	Recall (Class 0)	Recall (Class 1)	F1-Score (Class 0)	F1-Score (Class 1)	AUC	Specificity
ANN	0.842	0.893	0.700	0.892	0.702	0.892	0.701	0.917	0.89**2**
DT	0.845	0.894	0.707	0.895	0.705	0.894	0.706	0.91**9**	0.89**5**
RF	0.844	0.894	0.706	0.894	0.707	0.894	0.706	0.919	0.894
SVM	0.832	0.869	0.709	0.909	0.620	0.888	0.661	0.898	0.90**9**
Ensemble	0.843	0.881	0.722	0.909	0.658	0.895	0.689	0.918	0.909

Analysis of receiver operating characteristic curves

To evaluate the overall classification capability of the models, the AUC values derived from the receiver operating characteristic (ROC) curves were compared (Fig. 5). Tightly grouped curves across RF, DT, ANN, and the ensemble mirror their virtually uniform AUC scores (0.917–0.919), while the SVM curve tracks distinctly below them (AUC = 0.898).

Spatial cross-validation and ensemble configuration

Under spatially blocked cross-validation (Table 3), the AUC of all models decreased compared with the random test set, to 0.870 ± 0.023 for ANN, 0.866 ± 0.028 for the ensemble, 0.865 ± 0.021 for RF, 0.851 ± 0.038 for DT, and 0.842 ± 0.058 for SVM (mean ± standard deviation across folds). A drop of around 0.05–0.07 points to inflated accuracy estimates under random splitting when evaluated on geographically novel zones, echoing the spatial autocorrelation pattern noted by Roberts *et al.* (2017). Fold-by-fold leadership rotated across individual classifiers, RF topped fold 1, ANN topped folds 2–4, and SVM topped fold 5, whereas the ensemble placed second in four out of five folds and fourth in fold 1, staying clear of last place throughout. The observed flood rate in the validation folds ranged from 0.234 to 0.315. The block bootstrap showed that the AUC of the ensemble did not differ significantly from that of ANN (ΔAUC 95% confidence interval: -0.007 to 0.002) or RF (-0.002 to 0.007) but was significantly higher than that of DT (0.005 to 0.026) and SVM (0.012 to 0.064). The ensemble also had the lowest expected calibration error (0.049, compared with 0.061-0.074 for the single models) and a Brier score (0.135) similar to that of ANN. Regarding the ensemble configuration, AUC-based weighting produced weights of 0.234-0.260, which were nearly identical to equal weighting and yielded an almost identical AUC (0.864). Removing SVM lifted recall from 0.567 to 0.595, without improving AUC (0.863), while pushing expected calibration error up to 0.061 and expanding false positives from 35,250 to 37,751. Equal-weight soft voting of all four models was therefore retained. At the 0.5 threshold, the spatially validated ensemble had a recall of 0.567 and a specificity of 0.875; lowering the threshold to 0.3 increased recall to 0.825 but raised the number of false positives from 35,250 to 65,836 parcels. Shifting the classification cutoff provides a practical lever when under-detecting flood-prone parcels is costlier than triggering false alarms. Such behavior helps explain why ensembling fell short of beating the strongest individual models: RF, DT, and ANN delivered comparable discrimination and closely matching predictions, reaching identical class assignments

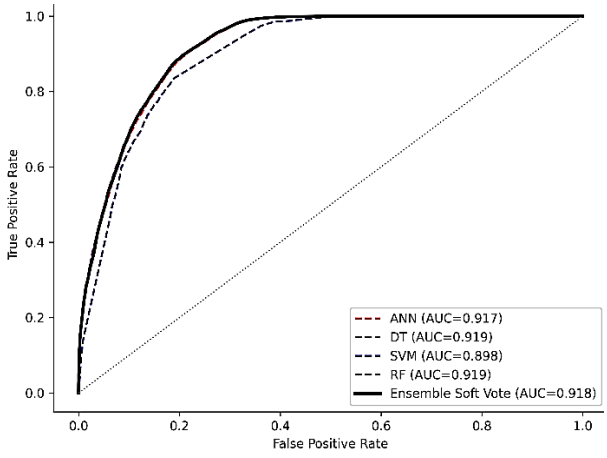

Fig. 5: Comparison of receiver operating characteristic curves of the five models

Table 3: Performance under spatially blocked five-fold cross-validation (2 km blocks); AUC is the mean ± standard deviation across folds, and the other metrics were calculated from pooled out-of-fold predictions at a threshold of 0.5

Model	AUC (fold mean ± standard deviation)	Pooled AUC	Precision	Recall	Specificity	F1-Score	Brier	ECE
ANN	0.870 ± 0.023	0.867	0.617	0.591	0.868	0.604	0.135	0.061
DT	0.851 ± 0.038	0.850	0.596	0.590	0.856	0.593	0.145	0.074
RF	0.865 ± 0.021	0.862	0.612	0.589	0.866	0.600	0.138	0.061
SVM	0.842 ± 0.058	0.830	0.609	0.487	0.887	0.541	0.149	0.064
Ensemble (equal weights)	0.866 ± 0.028	0.864	0.620	0.567	0.875	0.592	0.135	0.049
Ensemble (AUC-weighted)	–	0.864	0.620	0.567	0.875	0.592	0.135	0.050
Ensemble (without SVM)	–	0.863	0.615	0.595	0.866	0.605	0.137	0.061

across reaching identical class assignments across all four learners on 90.0% of parcels; which restricts how much AUC can gain from blending nearly redundant probability scores. Under spatial validation, the main contribution of soft voting was instead a more stable ranking across regions and better-calibrated probabilities, which is relevant because the susceptibility levels are derived directly from the averaged probability. Table 4 compares the present results with those of the previous studies cited in this study.

Flood susceptibility map

Evaluation outcomes supported selecting the ensemble surface for the final flood susceptibility map: stronger precision and fewer false alarms limit mistaken susceptibility flags on non-flooded parcels, while probability calibration under spatial cross-validation outpaced the individual learners, even though positive recall trailed RF, DT, and ANN. The map presents the soft voting probability for each land parcel (Fig. 6). Under spatial cross-validation (out-of-fold predictions), the observed 2024 flood rate increased consistently from the Very Low to the Very High level (5.3%, 38.5%, 52.7%, 60.7%, and 68.7%). Of the parcels flooded in 2024, 46.4% were classified as High or Very High, whereas 10.8% were classified as Very Low; conversely, 70.0% of the non-flooded parcels were classified as Very Low. The predicted probabilities overestimated the observed flood rate at the upper end (mean predicted probability of 0.89 compared with an observed rate of 0.69 in the Very High level), confirming that the levels indicate relative rather than absolute susceptibility. Model divergence clustered in the Moderate susceptibility band, with all four learners sharing the same class label on merely 42.2% of parcels, indicating substantial disagreement in intermediate-risk areas.

Table 4: Comparison of the present study with previous flood-related machine learning studies cited in this paper

Study	Study area and flood data	Conditioning factors	Algorithms	Validation	Reported performance	Limitations
Choubin *et al*. (2019)	Khiyav-Chai watershed, Iran; 51 recorded flood locations from the regional water agency and 51 non-flood points	11 (altitude, slope, aspect, curvature, distance from river, topographic wetness index, drainage density, soil depth, soil hydrological groups, land use, lithology)	Multivariate discriminant analysis, classification and regression trees, and SVM; AUC-weighted ensemble	Random 70:30 split	Ensemble AUC = 0.91 (single models 0.83-0.89)	Shortage of recorded flood locations
Duwal *et al*. (2023)	Karnali River Basin, Nepal; 424 flood and non-flood points (equal numbers) from the national disaster portal and Sentinel-1 flood mapping	10 (aspect, curvature, distance to river, normalized difference vegetation index, elevation, slope, rainfall, soil, stream power index, topographic wetness index)	ANN, SVM, and RF	Random 70:30 split; 15-fold cross-validation on the training data	AUC (prediction rate) = 0.987 for SVM, 0.985 for RF, and 0.981 for ANN	–
Saleh *et al*. (2024)	Qaa'Jahran Basin, Yemen; 141 flood and 141 non-flood locations from SAR imagery (2005, 2006, 2020, and 2022 events) and historical data	15 initial factors, reduced to elevation and distance to streams by metaheuristic feature selection	Bagging, boosting, and stacking ensembles of SVM, k-nearest neighbors, and DT	Random 80:20 split	Boosting ensemble: accuracy = 98.75%, AUC = 0.990	Higher computational complexity; transferability to other regions not yet tested
Abdo *et al*. (2025)	Baniyas River basin, Syria; 1,100 flood locations from historical records (1991-2023) and 1,100 non-flood locations supported by fieldwork	20 flood-driving factors	SVM, RF, ANN, and extreme gradient boosting	Random 70:30 split; 10-fold cross-validation	AUC = 0.98 for extreme gradient boosting and RF, 0.97 for ANN, and 0.94 for SVM	Difficulty in obtaining factor data; fieldwork constraints
Rahman *et al*. (2025)	Kabul River Basin, Eastern Hindu Kush; 570 flooded and 570 non-flooded locations from news reports, literature, field surveys, and satellite imagery	16 topographical, hydrological, vegetational, and environmental predictors	Logistic regression, ANN, extreme gradient boosting, RF, k-nearest neighbors, and naive Bayes	Training and testing datasets (success and prediction rate curves)	AUC (prediction rate) = 0.983 for extreme gradient boosting and 0.980 for RF	Potential overfitting of tree-based models; sensitivity to training data quality
This study	Chiang Mai Comprehensive Plan area, Thailand; 383,208 land parcels labeled from 4,711 field-surveyed flood marks (2024 event)	5 (land use, land cover, elevation, slope, distance to river)	ANN, SVM, DT, RF; equal-weight soft voting	Stratified random 80:20 split with 5-fold cross-validation; spatially blocked 5-fold cross-validation (2 km blocks)	Random test set: AUC = 0.898-0.919; spatially blocked cross-validation: AUC = 0.842-0.870; ensemble comparable to ANN and RF and best calibrated	Single flood event; no rainfall or hydrological variables; centroid-based labeling

Performance values are as reported in each study and are not directly comparable because the studies differ in study area, flood data, and validation method.

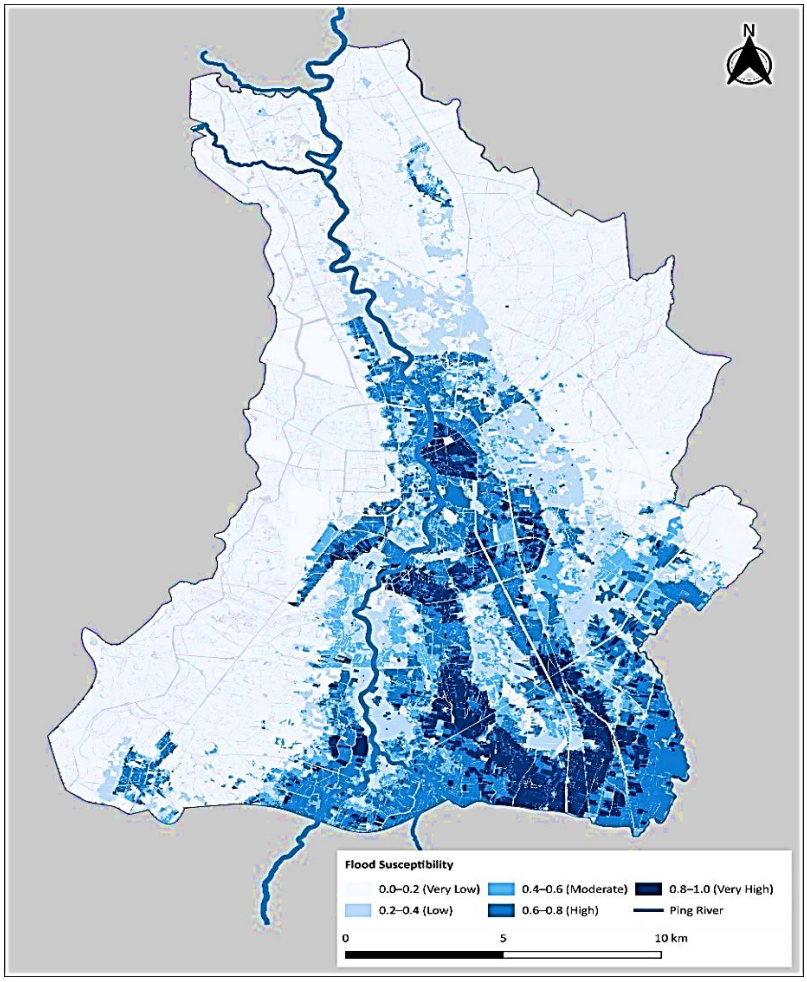

Fig. 6: Flood susceptibility map generated by ensemble soft voting (susceptibility gradient 0.0-1.0)

Feature importance analysis

Table 5 presents the feature importance analysis, evaluated through model-agnostic permutation tests (AUC decrease on the independent test set) and native tree metrics (MDI/Gini). Elevation (X3) led all four algorithms as the top conditioning variable, cutting permutation AUC by more than 0.31 in every model while supplying roughly half of tree-based split importance (RF MDI = 0.520, DT Gini = 0.502). This consistency across tree-based (DT, RF), kernel-based (SVM), and neural network (ANN) approaches strengthens confidence in the identified importance ranking, as it is unlikely to be an artifact of any single model's inductive bias. However, both permutation and impurity-based measures quantify the contribution of each factor to model predictions and do not constitute evidence of physical causation or establish direct mechanistic relationships between variables. Elevation's top ranking echoes Gohil *et al.* (2024), who pointed to elevation as a vital determinant since low-lying ground often aligns with floodplains and basin landform. Beyond elevation, the tree-based models (RF, DT) and SVM identified Land Use (X1) as the second most influential variable (importance ~0.129-0.163; SVM = 0.140), closely followed by Distance to River (X5) (~0.123-0.143; SVM = 0.133). Conversely, the ANN model prioritized Distance to River (X5: 0.134) marginally

Table 5: Feature importance of flood conditioning factors from permutation tests and native tree metrics

Feature	Permutation importance (AUC decrease)				Native tree importance	
	RF	DT	ANN	SVM	RF (MDI)	DT (Gini)
Elevation (X3)	0.317 ± 0.002	0.343 ± 0.002	0.315 ± 0.002	0.315 ± 0.005	0.520	0.502
Land use (X1)	0.129 ± 0.001	0.163 ± 0.001	0.127 ± 0.001	0.140 ± 0.003	0.243	0.225
Distance to river (X5)	0.123 ± 0.002	0.143 ± 0.002	0.134 ± 0.002	0.133 ± 0.003	0.193	0.211
Slope (X4)	0.018 ± 0.000	0.022 ± 0.000	0.012 ± 0.000	0.014 ± 0.001	0.030	0.041
Land cover (X2)	0.006 ± 0.000	0.008 ± 0.000	0.006 ± 0.000	0.009 ± 0.001	0.014	0.021

above Land Use (X1: 0.127). Although their relative ranks differ marginally, these two predictors maintain a steady, secondary level of influence in every model tested (importance ranging from 0.12 to 0.16). The importance of land use is consistent with Rentschler *et al.* (2023), who reported that development in flood-prone areas increases the concentration of susceptible locations, and the importance of distance to river agrees with Saleh *et al.* (2024). In contrast, Slope (X4) and Land Cover (X2) exhibited minimal influence across all configurations (permutation values < 0.025), a pattern potentially attributable to the predominantly flat basin morphology of the urban study extent, where elevation gradients and proximity to the main discharge channel may primarily govern hydraulic flow. Topographic relief and flow behavior across the Chiang Mai basin may help explain why slope (X4) and land cover (X2) play a comparatively minor predictive role. First, the minimal contribution of Slope (importance ≤ 0.022 across all four models) likely reflects the flat topography across the urban core and contiguous lowlands. Limited slope variability across the study area restricts the models' ability to differentiate flood-prone parcels from unaffected ones. Gravitational surface runoff and inundation depth may instead be governed mainly by absolute low points (Elevation, X3) and lateral river overflow (Distance to River, X5). This inference aligns with Gohil *et al.* (2024), who observed that low-relief topography impedes drainage and emphasized evaluating slope jointly with elevation. Second, Land Cover (X2) has negligible influence (importance ≤ 0.009 across all four models), likely because surface permeability is largely superseded by topographic elevation and gravitational accumulation in this basin setting. Although pervious land cover theoretically aids water infiltration (Tang *et al.*, 2024), natural retention areas and agricultural lands within the Chiang Mai floodplain predominantly occupy lower baseline elevations. Under intense rainfall events, runoff sheds from adjacent uplands and collects in these low-lying basins. When the Ping River reaches or breaches bankfull levels, sustained high water stages saturate the ground and drive widespread inundation across the lowlands, overriding local differences in surface permeability. Consequently, surface infiltration capacity becomes less relevant once regional overbank accumulation submerges an area, making Elevation (X3) and development zoning (Land Use, X1) more decisive than generalized land cover categories. A similar pattern was reported by Narendra *et al.* (2024), who found that flooding still occurred in watersheds with good forest cover because watershed geomorphometric characteristics strongly influenced flood events. Rather than reflecting direct empirical measurements from a standalone hydrological investigation, these mechanisms are offered as physically plausible inferences aligned with the modeling outcomes. To align the feature importance evaluation with spatial predictive outcomes, the ensemble soft voting results were assessed across five susceptibility levels (Very Low: 0.000-0.200, Low: 0.200-0.400, Moderate: 0.400-0.600, High: 0.600-0.800, and Very High: 0.800-1.000) alongside local geographic and

morphological characteristics. Across the Chiang Mai Comprehensive Plan area, high-susceptibility parcels cluster spatially rather than appearing at random, reflecting elevation gradients and built-up density in line with the top-ranked predictors from the permutation importance results. Very Low susceptibility (0.000-0.200): Land parcels in this level are predominantly distributed across the outer periphery of the comprehensive plan boundary, generally corresponding to relatively elevated terrain at the basin margins. In terms of statutory land use, this level is dominated by low-density residential land (yellow zone: 53.35%) and rural and agricultural land (green zone: 19.01%), with commercial nodes (red zone: 11.60%) and medium-density sectors (orange zone: 11.59%) playing secondary roles. In the study area, low-density residential and rural parcels are more commonly situated on higher ground away from the main Ping River channel, reinforcing the role of elevation and channel proximity highlighted by the feature importance results. Low susceptibility (0.200-0.400): This level functions as an intermediate transition zone separating expanding suburban developments from the low-lying urban core. Spatially, low-density residential land (yellow zone) continues to comprise the majority at 48.50%, supplemented by rural and agricultural land (green zone: 17.27%) and commercial parcels (red zone: 18.27%), while medium-density development (orange zone) accounts for only 5.69%. Several parcels along parts of the Ping River nonetheless fall into this lower-susceptibility class, showing that proximity to the channel does not automatically confer high risk. Local relief likely offsets channel closeness in these zones, a localized anomaly that merits targeted, site-scale hydrological analysis outside the scope of this study. Moderate susceptibility (0.400-0.600): Although distributed across multiple areas within the study extent, this level is predominantly clustered in low-lying basin sectors and remains in moderate proximity to the Ping River corridor. Zonal cross-tabulation shows a contraction of low-density residential land to 43.47%, offset by an increase in medium-density residential land (orange zone: 19.88%), alongside sustained shares of rural and agricultural land (green zone: 17.50%) and commercial land (red zone: 15.48%). Moving from the Low and Very Low classes toward higher-susceptibility zones coincides with denser urban development, lower elevations, and shorter distances to the river, matching the feature importance gradient. However, the present study did not directly model the hydraulic mechanisms underlying this transition (e.g., localized drainage capacity). High susceptibility (0.600-0.800): Covering extensive continuous areas adjacent to the primary embankments of the Ping River, this level is heavily concentrated across low-lying floodplain areas near the river corridor. Correspondingly, land allocations shift toward heavily built classifications: medium-density residential land (orange zone) peaks as the dominant class at 36.77%, and commercial land (red zone) expands to 24.85% (collectively representing 61.62% of the level), while low-density residential areas contract sharply to 11.68%, and rural and agricultural land accounts for 22.36%. Compared with the Moderate class, this higher tier intensifies the overlap of lower elevations, greater river proximity, and denser urban development, reflecting a broader pattern in which urban growth extends into low-lying flood-exposed areas (Rentschler *et al.*, 2023). Very High susceptibility (0.800-1.000): Parcels in this level form distinct clusters that do not strictly follow the continuous embankments of the main Ping River; instead, they concentrate in low-lying areas across the southern and eastern portions of the study extent. Occupying the lowest relative elevations across all classes, these parcels reinforce the elevation-based susceptibility gradient observed

across the study. In terms of statutory land use, rural and agricultural land (green zone: 32.33%) and medium-density residential land (orange zone: 26.86%) form the majority, complemented by cultural conservation zones (light brown zone: 15.34%) and regulated residential overlays (yellow hatched zone: 14.16%). This level contains the highest combined share of rural and agricultural (green) and cultural conservation (light brown) zones among the five levels, indicating that some agricultural and heritage-designated areas within the comprehensive plan boundary coincide with the highest susceptibility level, which may warrant attention in land-use and heritage planning. Overall, the spatial pattern derived from ensemble soft voting aligns with Elevation, Distance to River, and Land Use as the key conditioning factors for flood susceptibility in the Chiang Mai basin. Moving inward from elevated outer margins toward low-lying riverfront zones, flood susceptibility typically rises alongside greater residential concentration. This multi-level classification therefore offers a preliminary evidence base for relevant stakeholders and planning authorities. It can help prioritize site-specific investigation in high and very high susceptibility areas, especially where dense residential or heritage-designated land uses are present, before making further urban development decisions in these areas.

CONCLUSION

This study developed a flood susceptibility assessment framework for the Chiang Mai Comprehensive Plan area by comparing ANN, SVM, DT, and RF and integrating them through ensemble soft voting. Binary inundation labels were assigned across 383,208 land parcels using 2024 field-surveyed flood extents to establish ground-truth data for model training and evaluation. On the independent test set, RF, DT, ANN, and the ensemble achieved comparable discrimination (AUC 0.917-0.919), whereas SVM achieved a lower AUC of 0.898. Under spatially blocked cross-validation, AUC decreased to 0.842-0.870, indicating that random splitting overestimated performance for spatially unseen areas; the ensemble did not differ significantly from ANN and RF, outperformed DT and SVM, ranked second in four of five folds, and produced the best-calibrated probabilities. Model behavior varied markedly across classifiers: RF, DT, and ANN captured a larger share of flood-susceptible parcels through higher recall, whereas the ensemble prioritized reliability, delivering peak precision (0.722), SVM-level specificity (0.909), and minimal false positives, while trading off recall (0.658). Feature importance evaluations identified Elevation (X3) as the primary conditioning factor across all models, followed by Land Use (X1) and Distance to River (X5). Slope (X4) and Land Cover (X2) had minimal influence (permutation importance ≤ 0.022 across all four models), likely reflecting the flat terrain of the Chiang Mai urban basin, where slope exhibits little spatial variation and is therefore less useful for distinguishing flood-prone from non-flood-prone parcels. Across the five susceptibility classes, flood susceptibility rises from higher outer margins toward low-lying areas near the Ping River, where medium-density residential and commercial areas account for a prominent concentration of high susceptibility. The flood susceptibility map can serve as a parcel-level screening tool for local authorities and urban planners within the Chiang Mai Comprehensive Plan area, helping to prioritize zones for detailed hydraulic modeling and site investigation before zoning or infrastructure decisions are made, rather than serving as a stand-alone flood risk assessment. For spatial planning, the five-class map offers a practical screening tool to target areas for site-level evaluation ahead of major development commitments. Selecting a specific model can then be tailored to operational goals,

balancing broader identification of flood-susceptible parcels against fewer redundant field assessments. A principal contribution of this study lies in integrating field-verified inundation observations with parcel-level susceptibility modeling, thereby aligning spatial predictions with the administrative unit at which zoning regulations and land-development decisions are enacted. In addition, the spatially blocked validation showed that the main advantage of soft voting was stability and calibration rather than higher discrimination. This study has several limitations. The model relies on static physical parameters (Elevation, Slope, Distance to River, Land Use, and Land Cover) without dynamic rainfall time series or climate projections as input variables. It therefore reflects baseline physical susceptibility derived from the 2024 flood event and does not account for potential shifts in flood susceptibility driven by future climate change. Several methodological constraints also warrant consideration when interpreting the results. Training on a single flood episode means the predictions may partially capture event-specific conditions, while 30-meter elevation resampling and centroid-based parcel representation can smooth out fine-scale variation within extensive parcels. Furthermore, hydrological variables such as rainfall intensity, drainage density, soil characteristics, and flow accumulation were not included, the predicted values are not calibrated probabilities, and 10.8% of the parcels flooded in 2024 were assigned to the Very Low level under spatial cross-validation. Future urban growth is expected to have negligible impact on Elevation (X3), Distance to River (X5), and Slope (X4), as these are physically static variables, whereas urban expansion primarily alters Land Use (X1) and, to a lesser extent, Land Cover (X2). Periodic model retraining is advisable whenever statutory zoning undergoes major expansion or reclassification, or when urban growth alters underlying land-use conditions. Furthermore, application to other geographic areas requires retraining with local spatial data layers and site-specific flood inventories, as the current model parameters are calibrated to the physical and statutory land-use characteristics of the Chiang Mai Comprehensive Plan area. Subsequent investigations should integrate time-varying rainfall and hydrological covariates, multi-event inundation inventories, and validation with independent flood events to rigorously evaluate spatial and temporal model transferability.

AUTHOR CONTRIBUTIONS

S. Sitthikankun conceptualized the study, developed the methodology and software, performed the formal analysis, prepared the visualizations, and wrote the original draft of the manuscript. N. Suriyanon validated the results and reviewed and edited the manuscript. C. Aryupong provided resources, curated the data, and reviewed and edited the manuscript. D. Rinchumphu, the corresponding author, conceptualized the study, supervised the research, administered the project, and reviewed and edited the manuscript.

CONFLICT OF INTEREST

The authors declare that there is no conflict of interests regarding the publication of this manuscript. In addition, the ethical issues, including plagiarism, informed consent, misconduct, data fabrication and/or falsification, double publication and/or submission, and redundancy have been completely observed by the authors.

OPEN ACCESS

©2027 The author(s). This article is licensed under a Creative Commons Attribution 4.0 International License, which permits use, sharing, adaptation, distribution and reproduction in any

medium or format, as long as you give appropriate credit to the original author(s) and the source, provide a link to the Creative Commons license, and indicate if changes were made. The images or other third-party material in this article are included in the article's Creative Commons license, unless indicated otherwise in a credit line to the material. If material is not included in the article's Creative Commons license and your intended use is not permitted by statutory regulation or exceeds the permitted use, you will need to obtain permission directly from the copyright holder. To view a copy of this license, visit: http://creativecommons.org/licenses/by/4.0/

PUBLISHER'S NOTE

GJESM Publisher remains neutral regarding jurisdictional claims in published maps and institutional affiliations.

POSITIVE AI STATEMENT

During the preparation of this work the authors used Artificial Intelligence (AI) tools, Gemini (Google) and Claude (Anthropic), to improve the language and readability of the manuscript, to assist in restructuring it to the journal format, and to assist in creating the graphical abstract. After using these tools, the authors reviewed and edited the content as needed and take full responsibility for the content of the publication.

ABBREVIATIONS

%	Percent
ANN	Artificial neural network
AUC	Area under the receiver operating characteristic curve
Class 0	Non-flooded parcel
Class 1	Flooded parcel
df	Degrees of freedom (number of dummy variables of a categorical factor)
DEM	Digital elevation model
DT	Decision tree
ECE	Expected calibration error
e.g.	Exempli gratia (for example)
Eq.	Equation
FCNN	Fully convolutional neural network
Fig.	Figure
GDAL/OGR	Geospatial data abstraction library / OGR simple features library
GEE	Google Earth Engine
GIS	Geographic information system
GPS	Global positioning system
GVIF	Generalized variance inflation factor
ID	Identifier
km	Kilometer
MCC	Matthews correlation coefficient
MDI	Mean decrease in impurity
ML	Machine learning
n	Number of samples
N	Number of base models
NASADEM	National Aeronautics and Space Administration digital elevation model
Pi(x)	Predicted flood probability of the i-th base model
Psoft(x)	Ensemble soft voting probability
PRISMA	Preferred reporting items for
QGIS	Quantum geographic information system
RBF	Radial basis function
RF	Random forest
ROC	Receiver operating characteristic
SAR	Synthetic aperture radar
SVM	Support vector machine
UAV	Unmanned aerial vehicle
VIF	Variance inflation factor
x	Feature vector
X1	Land use
X2	Land cover
X3	Elevation
X4	Slope
X5	Distance to river
Y	Binary target variable (flooded or non-flooded)

REFERENCES

Abdo, H.G.; Richi, S.M.; Zeng, T.; Alqadhi, S.; Prasad, P.; Nguyen-Huy, T.; Alharbi, M.M.; Mallick, J., (2025). Machine learning-based assessment of flood susceptibility in the Eastern Mediterranean: A case study of Baniyas River basin. Geomatics Nat. Hazards Risk. 16(1): 2524417 **(28 pages).**

Abraham, M.T.; Satyam, N.; Lokesh, R.; Pradhan, B.; Alamri, A., (2021). Factors affecting landslide susceptibility mapping: Assessing the influence of different machine learning approaches, sampling strategies and data splitting. Land. 10(9): 989 **(24 pages).**

Abu-Salih, B.; Wongthongtham, P.; Coutinho, K.; Qaddoura, R.; Alshaweesh, O.; Wedyan, M., (2023). The development of a road network flood risk detection model using optimised ensemble learning. Eng. Appl. Artif. Intell., 122: 106081 **(21 pages).**

Alexopoulos, M.J.; Iliopoulou, T.; Modé, P.; Istrati, D.; Koutsoyiannis, D.; Królewicz, S.; Graf, R.; Kaczmarek, L.; Rączkowski, W., (2025). Flood risk assessment of cultural heritage sites near lakes via advanced hydrodynamic modeling and digital technologies. Results Eng., 28: 107977 **(19 pages).**

Bentivoglio, R.; Isufi, E.; Jonkman, S.N.; Taormina, R., (2022). Deep learning methods for flood mapping: A review of existing applications and future research directions. Hydrol. Earth Syst. Sci., 26(16): 4345-4378 **(34 pages).**

Bhattarai, Y.; Duwal, S.; Sharma, S.; Talchabhadel, R., (2024). Leveraging machine learning and open-source spatial datasets to enhance flood susceptibility mapping in transboundary river basin. Int. J. Digital Earth. 17(1): 2313857 **(24 pages).**

Brown, C.F.; Brumby, S.P.; Guzder-Williams, B.; Birch, T.; Hyde, S.B.; Mazzariello, J.; Czerwinski, W.; Pasquarella, V.J.; Haertel, R.; Ilyushchenko, S.; Schwehr, K.; Weisse, M.; Stolle, F.; Hanson, C.; Guinan, O.; Moore, R.; Tait, A.M., (2022). Dynamic World, near real-time global 10 m land use land cover mapping. Sci. Data. 9(1): 251 **(17 pages).**

Center of Excellence in Natural Disaster Management, (2024). CM flood mark 2024. Chiang Mai University.

Choubin, B.; Moradi, E.; Golshan, M.; Adamowski, J.; Sajedi-Hosseini, F.; Mosavi, A., (2019). An ensemble prediction of flood susceptibility using multivariate discriminant analysis, classification and regression trees, and support vector machines. Sci. Total Environ., 651: 2087-2096 **(10 pages).**

Chowdhuri, I.; Pal, S.C.; Chakrabortty, R., (2020). Flood susceptibility mapping by ensemble evidential belief function and binomial logistic regression model on river basin of eastern India. Adv. Space Res., 65(5): 1466-1489 **(24 pages).**

Crippen, R.; Buckley, S.; Agram, P.; Belz, E.; Gurrola, E.; Hensley, S.; Kobrick, M.; Lavalle, M.; Martin, J.; Neumann, M., (2016). NASADEM global elevation model: Methods and progress. Int. Arch. Photogramm. Remote Sens. Spatial Inf. Sci., 41: 125-128 **(4 pages).**

Damayanti, H.N.; Wikan, P.A.; Annurhutami, F., (2024). GIS-based flood susceptibility mapping in Wawar Watershed, Purworejo Regency. IOP Conference Series: Earth Environ. Sci., 1314(1): 012051 **(14 pages).**

Dharmarathne, G.; Waduge, A.O.; Bogahawaththa, M.; Rathnayake, U.; Meddage, D.P.P., (2024). Adapting cities to the surge: A comprehensive review of climate-induced urban flooding. Results Eng., 22: 102123 **(15 pages).**

Duwal, S.; Liu, D.; Pradhan, P.M., (2023). Flood susceptibility modeling of the Karnali river basin of Nepal using different machine learning approaches. Geomatics Nat. Hazards Risk. 14(1): 2217321 **(25 pages).**

Ekmekcioğlu, Ö.; Koc, K.; Özger, M.; Işık, Z., (2022). Exploring the additional value of class imbalance distributions on interpretable flash flood susceptibility prediction in the Black Warrior River basin, Alabama, United States. J. Hydrol., 610: 127877 **(18 pages).**

Faksomboon, B.; Khamcharoen, N.; Keoviyavong, T., (2025). Modeling hydrological impacts of land-use change in the Sam Ngao Watershed using SWAT and CA-Markov. Nakhara: J. Environ. Des. Plann., 24(3): Article 518 **(25 pages).**

Fox, J.; Monette, G., (1992). Generalized collinearity diagnostics. J. Am. Stat. Assoc., 87(417): 178-183 **(6 pages).**

Gohil, M.; Mehta, D.; Shaikh, M., (2024). An integration of geospatial and fuzzy-logic techniques for flood-hazard mapping. J. Earth Syst. Sci., 133(2): 80 **(16 pages).**

Gu, Z.; Phakdimek, S.; Nagami, K.; Komori, D., (2025). Relationship between urbanization-induced land use changes and flood risk: Case study in Chiang Mai, Thailand. Water. 17(3): 327 **(20 pages).**

Hong, H.; Panahi, M.; Shirzadi, A.; Ma, T.; Liu, J.; Zhu, A.X.; Chen, W.; Kougias, I.; Kazakis, N., (2018). Flood susceptibility assessment in Hengfeng area coupling adaptive neuro-fuzzy inference system with genetic algorithm and differential evolution. Sci. Total Environ., 621: 1124-1141 **(18 pages).**

Hongnual, K.; Leelapattana, W.; Thongma, W.; Trakansiriwanich, K.; Sitthikun, S., (2021). The development of cultural tourism attraction for model creative tourism management in the old city Chiang Mai, Thailand. J. Manage. Inf. Decis. Sci., 24: 1-8 **(8 pages).**

Intarat, K.; Yoomee, P.; Hussadin, A.; Lamprom, W., (2024). Assessment of landslide susceptibility in the intermontane basin area of northern Thailand. Environ. Nat. Resour. J., 22(2): 158-170 **(13 pages).**

Khalid, R.; Khan, U.T., (2024). Flood susceptibility mapping using ANNs: A case study in model generalization and accuracy from Ontario, Canada. Geocarto Int., 39(1): 2316653 **(30 pages).**

Khosravi, K.; Shahabi, H.; Pham, B.T.; Adamowski, J.; Shirzadi, A.; Pradhan, B.; Dou, J.; Ly, H.-B.; Gróf, G.; Ho, H.L.; Hong, H.; Chapi, K.; Prakash, I., (2019). A comparative assessment of flood susceptibility modeling using multi-criteria decision-making analysis and machine learning methods. J. Hydrol., 573: 311-323 **(13 pages).**

Khudhair, Z.S.; Zubaidi, S.L.; Dulaimi, A.; Al-Bugharbee, H.; Muhsen, Y.R.; Putra Jaya, R.; Ridha, H.M.; Raza, S.F.; Ethaib, S., (2024). Metaheuristic algorithms applied in ANN salinity modelling. Results Eng., 23: 102541 **(10 pages).**

Krishnachaithanya, N.; Bagavathi Sivakumar, P.; Deepika, T., (2025). Probabilistic flood risk mapping for Indian megacities using a scalable machine learning framework in Google Earth Engine. Results Eng., 28: 107872 **(12 pages).**

Leelawat, N.; Laosunthara, A.; Srivichai, M.; Sararit, T.; Kodaka, A.; Tungkasikij, N.; Saengtabtim, K.; Kohtake, N.; Tang, J., (2025). The 2024 northern Thailand floods: A preliminary disaster report. J. Disaster Res., 20: sc20250319 **(8 pages).**

Ministry of Interior, (2012). Ministerial regulation enforcing the comprehensive plan of Chiang Mai City (3rd revision), B.E. 2555 (2012). Royal Thai Government Gazette. 129(44A). (In Thai)

Narendra, B.H.; Setiawan, O.; Hasan, R.A.; Siregar, C.A.; Pratiwi; Sari, N.; Sukmana, A.; Dharmawan, I.W.S.; Nandini, R., (2024). Flood susceptibility mapping based on watershed geomorphometric characteristics and land use/land cover on a small island. Global J. Environ. Sci. Manage., 10(1): 301-320 **(20 pages).**

Nguyen Van, L.; Lee, G., (2025). Optimizing stacked ensemble machine learning models for accurate wildfire severity mapping. Remote Sens., 17(5): 854 **(18 pages).**

Notti, D.; Giordan, D.; Caló, F.; Pepe, A.; Zucca, F.; Galve, J.P., (2018). Potential and limitations of open satellite data for flood mapping. Remote Sens., 10(11): 1673 **(30 pages).**

Panyadee, P.; Champrasert, P., (2024). Spatiotemporal flood hazard map prediction using machine learning for a flood early warning case study: Chiang Mai Province, Thailand. Sustainability. 16(11): 4433 **(19 pages).**

Pradhan, B.; Lee, S.; Dikshit, A.; Kim, H., (2023). Spatial flood susceptibility mapping using an explainable artificial intelligence (XAI) model. Geosci. Front., 14(6): 101625 **(12 pages).**

Prasertsoong, N.; Puttanapong, N., (2025). Urban land expansion and economic development in Thailand from 2000 to 2020. Nakhara: J. Environ. Des. Plann., 24(3): Article 517 **(37 pages).**

Puno, G.R.; Puno, R.C.C.; Maghuyop, I.V., (2021). Two-dimensional flood model for risk exposure analysis of land use/land cover in a watershed. Global J. Environ. Sci. Manage., 7(2): 225-238 **(14 pages).**

Puno, G.R.; Puno, R.C.C.; Maghuyop, I.V., (2022). Flood hazard simulation and mapping using digital elevation models with different resolutions. Global J. Environ. Sci. Manage., 8(3): 339-352 **(14 pages).**

Rachmawardani, A.; Kurniawan, B.; Wijaya, S.K.; Sopaheluwakan, A.; Sinambela, M., (2025). Hybrid machine learning for flood prediction: Comparing CHIRPS satellite and ground station data. J. Water Land Dev., 64: 87-99 **(13 pages).**

Rahman, Z.U.; Zhang, M.; Chen, F.; Ullah, S.; Ahmad, M.; Feroz, A.; Danhassan, S.S.; Azzam, A., (2025). Flood susceptibility mapping using supervised machine learning models: Insights into predictors' significance and models' performance. Geomatics Nat. Hazards Risk. 16(1): 2516728 **(26 pages).**

Rahmati, O.; Kornejady, A.; Samadi, M.; Deo, R.C.; Conoscenti, C.; Lombardo, L.; Dayal, K.; Taghizadeh-Mehrjardi, R.; Pourghasemi, H.R.; Kumar, S.; Bui, D.T., (2019). PMT: New analytical framework for automated evaluation of geo-environmental modelling approaches. Sci. Total Environ., 664: 296-311 **(16 pages).**

Rentschler, J.; Avner, P.; Marconcini, M.; Su, R.; Strano, E.; Vousdoukas, M.; Hallegatte, S., (2023). Global evidence of rapid urban growth in flood zones since 1985. Nature. 622(7981): 87-92 **(6 pages).**

Roberts, D.R.; Bahn, V.; Ciuti, S.; Boyce, M.S.; Elith, J.; Guillera-Arroita, G.; Hauenstein, S.; Lahoz-Monfort, J.J.; Schröder, B.; Thuiller, W.; Warton, D.I.; Wintle, B.A.; Hartig, F.; Dormann, C.F., (2017). Cross-validation strategies for data with temporal, spatial, hierarchical, or phylogenetic structure. Ecography, 40(8): 913-929 **(17 pages).**

Saleh, A.R.; Al-Areeq, A.M.; Al Aghbari, A.A.; Ghaleb, M.; Benaafi, M.; Al-Areeq, N.M.; M. Al-Ramadan, B., (2024). A novel voting ensemble model empowered by metaheuristic feature selection for accurate flash flood susceptibility mapping. Geomatics Nat. Hazards Risk. 15(1): 2360000 **(29 pages).**

Seydi, S.T.; Kanani-Sadat, Y.; Hasanlou, M.; Sahraei, R.; Chanussot, J.; Amani, M., (2023). Comparison of machine learning algorithms for flood susceptibility mapping. Remote Sens., 15(1): 192 **(25 pages).**

Sitthikankun, S.; Chakarin, B.; Srivanit, M.; Rinchumphu, D., (2024). Identifying flood exposure factors of flooding prediction through spatial analysis and remote sensing. IWA 21st International Conference on Navigating Diffuse Pollution Pathways to Carbon Neutrality, Chiang Mai, Thailand. 11-14 December 2024.

Srivanit, M.; Pattanasri, S.; Phichetkunbodee, N.; Manokeaw, S.; Sitthikankun, S.; Rinchumphu, D., (2024). Analysis of sensitive urban form indicators of flood susceptible prediction based on machine learning models. Global J. Environ. Sci. Manage., 10(4): 1501-1518 **(18 pages).**

Talha, S.; Akhssas, A.; Aarab, A.; Aabi, A.; Berkat, B.; Amouch, S., (2025). Robust ensemble machine learning for flash flood susceptibility mapping across semiarid regions. Civ. Eng. J., 11(12): 4926-4960 **(35 pages).**

Tang, J.; Liu, D.; Shang, C.; Niu, J., (2024). Impacts of land use change on surface infiltration capacity and urban flood risk in a representative karst mountain city over the last two decades. J. Clean. Prod., 454: 142196 **(14 pages).**

Taromideh, F.; Fazloula, R.; Choubin, B.; Masoodi, M.; Mosavi, A., (2024). Ensemble machine learning for urban flood hazard assessment. 2024 IEEE 22nd World Symposium on Applied Machine Intelligence and Informatics (SAMI), 25-27 January 2024 **(6 pages).**

Tehrany, M.S.; Pradhan, B.; Jebur, M.N., (2014). Flood susceptibility mapping using a novel ensemble weights-of-evidence and support vector machine models in GIS. J. Hydrol., 512: 332-343 **(12 pages).**

Tochaiwat, K.; Pultawee, P., (2024). House type specification for housing development project using machine learning techniques: A study from Bangkok Metropolitan Region, Thailand. Nakhara: J. Environ. Des. Plann., 23(1): Article 403 **(16 pages).**

Tuganishuri, J.; Yune, C.Y.; Kim, G.; Lee, S.W.; Adhikari, M.D.; Yum, S.G., (2025). Prediction of the volume of shallow landslides due to rainfall using data-driven models. Nat. Hazards Earth Syst. Sci., 25(4): 1481-1499 (19 pages).

Usman Kaoje, I.; Abdul Rahman, M.Z.; Idris, N.H.; Razak, K.A.; Wan Mohd Rani, W.N.M.; Tam, T.H.; Mohd Salleh, M.R., (2021). Physical flood vulnerability assessment using geospatial indicator-based approach and participatory analytical hierarchy process: A case study in Kota Bharu, Malaysia. Water. 13(13): 1786 **(22 pages).**

Usman-Hamza, F.E.; Balogun, A.O.; Mamman, H.; Capretz, L.F.; Basri, S.; Oyekunle, R.A.; Mojeed, H.A.; Akintola, A.G., (2025). Empirical analysis of data sampling-based decision forest classifiers for software defect prediction. Software. 4(2): 7 **(34 pages).**

Verma, S.; Mehta, D.; Pandey, A.; Malani, S.; Pandey, R., (2024). Flood hazard: A QGIS plugin for assessing flood consequences. J. Water Manage. Model., 32 **(16 pages).**

Wang, H.; Meng, Y.; Xu, H.; Wang, H.; Guan, X.; Liu, Y.; Liu, M.; Wu, Z., (2024). Prediction of flood risk levels of urban flooded points though using machine learning with unbalanced data. J. Hydrol., 630: 130742 **(13 pages).**

Wara, S.S.M.; Nasrudin, M.; Adziima, A.F.; Pratama, A.R.; Damaliana, A.T.; Muhaimin, A., (2025). A weighted soft voting approach for classifying user comments on social welfare applications. 2025 IEEE 11th Information Technology International Seminar (ITIS), 8-10 October 2025 **(7 pages).**

Wienhold, K.J.; Li, D.; Li, W.; Fang, Z.N., (2023). Flood inundation and depth mapping using unmanned aerial vehicles combined with high-resolution multispectral imagery. Hydrology. 10(8): 158 **(24 pages).**

Wu, X.; Zhang, Z.; Xiong, S.; Zhang, W.; Tang, J.; Li, Z.; An, B.; Li, R., (2023). A near-real-time flood detection method based on deep learning and SAR images. Remote Sens., 15(8): 2046 **(20 pages).**

Wüthrich, D.; Korswagen, P.A.; Selvam, H.; Oetjen, J.; Bricker, J.; Schüttrumpf, H., (2025). Field survey assessment of flood loads and related building damage from the July 2021 event in the Ahr Valley (Germany). J. Flood Risk Manage., 18(1): e13024 **(23 pages).**

Yang, D.; Xiao, B.; Cao, M.; Shen, H., (2024). A new hybrid credit scoring ensemble model with feature enhancement and soft voting weight optimization. Expert Syst. Appl., 238: 122101 **(10 pages).**

Yaseen, Z.M., (2024). Flood hazards and susceptibility detection for Ganga river, Bihar state, India: Employment of remote sensing and statistical approaches. Results Eng., 21: 101665 **(20 pages).**

Yu, H.; Luo, Z.; Wang, L.; Ding, X.; Wang, S., (2023). Improving the accuracy of flood susceptibility prediction by combining machine learning models and the expanded flood inventory data. Remote Sens., 15(14): 3601 **(24 pages).**

Zhao, H.; Liu, W.; Wang, Y.; Wu, L., (2025). Comparative analysis of algorithmic approaches in ensemble learning: Bagging vs. boosting. Sci. Rep., 15(1): 34218 **(12 pages).**

AUTHOR (S) BIOSKETCHES

Sitthikankun, S., Ph.D. Candidate, Department of Civil Engineering, Faculty of Engineering, Chiang Mai University, 239 Huay Kaew Road, Suthep, Mueang, Chiang Mai 50200, Thailand.
- Email: *sitthikorn_sit@cmu.ac.th*
- ORCID: 0000-0001-6107-8010
- Web of Science ResearcherID: RMD-2010-2026
- Scopus Author ID: 57437092300
- Homepage: https://urbanintelligence.eng.cmu.ac.th/graduate-students/sitthikorn-sitthikankun/

Suriyanon, N., Ph.D., Associate Professor, Department of Civil Engineering, Faculty of Engineering, Chiang Mai University, 239 Huay Kaew Road, Suthep, Mueang, Chiang Mai 50200, Thailand.
- Email: *natee.suriyanon@cmu.ac.th*
- ORCID: 0009-0003-0669-4138
- Web of Science ResearcherID: RBQ-2458-2026
- Scopus Author ID: 54788469300
- Homepage: https://civil.eng.cmu.ac.th/?page_id=1096, https://urbanintelligence.eng.cmu.ac.th/experts/urban-management-experts/natee-suriyanon/

Aryupong, C., Associate Professor, Office of Research Administration, Chiang Mai University, 239 Huay Kaew Road, Suthep, Mueang, Chiang Mai 50200, Thailand.
- Email: *chuchoke.a@cmu.ac.th*
- ORCID: 0000-0002-5053-9800
- Web of Science ResearcherID: NA
- Scopus Author ID: 56703401600
- Homepage: https://tinyurl.com/3uyrxvvv

Rinchumphu, D., Ph.D., Associate Professor, Department of Civil Engineering, Faculty of Engineering, Chiang Mai University, 239 Huay Kaew Road, Suthep, Mueang, Chiang Mai 50200, Thailand.
- Email: *damrongsak.r@cmu.ac.th*
- ORCID: 0000-0002-6037-4974
- Web of Science ResearcherID: IUN-3065-2023
- Scopus Author ID: 57219602276
- Homepage: https://civil.eng.cmu.ac.th/?page_id=1096

HOW TO CITE THIS ARTICLE:
Sitthikankun, S.; Suriyanon, N.; Aryupong, C.; Rinchumphu, D., (2027). Flood susceptibility modeling of river overflow using an ensemble voting model. Global J. Environ. Sci. Manage.,13(2): ..._...

DOI: https://doi.org/10.22034/gjesm.2027.02.03
URL: https://www.gjesm.net/article_736438.html